

Aerobic and anaerobic methane oxidation in a seasonally anoxic basin

Herdís G. R. Steinsdóttir ,* Clemens Schauburger , Snehit Mhatre, Bo Thamdrup , Laura A. Bristow 

Department of Biology, University of Southern Denmark, Odense, Denmark

Abstract

Shallow coastal waters are dynamic environments that dominate global marine methane emissions. Particularly high methane concentrations are found in seasonally anoxic waters, which are spreading in eutrophic coastal systems, potentially leading to increased methane emissions to the atmosphere. Here we explore how the seasonal development of anoxia influenced methane concentrations, rates of methane oxidation, and the community composition of methanotrophs in the shallow eutrophic water column of Mariager Fjord, Denmark. Our results show the development of steep concentration gradients toward the oxic–anoxic interface as methane accumulated to 1.4 μM in anoxic bottom waters. Yet, the fjord possessed an efficient microbial methane filter near the oxic–anoxic interface that responded to the increasing methane flux. In experimental incubations, methane oxidation near the oxic–anoxic interface proceeded both aerobically and anaerobically with nearly equal efficiency reaching turnover rates as high as 0.6 and 0.8 d^{-1} , respectively, and was seemingly mediated by members of the Methylococcales belonging to the Deep Sea-1 clade. Throughout the period, both aerobic and anaerobic methane oxidation rates were high enough to consume the estimated methane flux. Thus, our results indicate that seasonal anoxia did not increase methane emissions.

Introduction

Atmospheric concentrations of methane—a major regulator of global climate—have increased nearly threefold from preindustrial levels (Saunois et al. 2020). Yet contemporary methane trends (1982–2020), including periods of stabilization (2000–2007) and renewed growth (2007–present), have thus far not been explained, demonstrating the need for resolving methane sources and sinks (Turner et al. 2019). Shallow coastal waters are estimated to contribute 50–80% of global marine methane emissions although they only cover 15% of the total ocean surface area (Weber et al. 2019). Particularly high concentrations of methane are observed in oxygen-depleted waters (Reeburgh et al. 1991; Sansone et al. 2001; Capelle et al. 2019). Since the mid-20th century, declining oxygen levels have been

recorded in coastal seas, bays, and estuaries such as the Baltic Sea, Chesapeake Bay, and the Danish coastal zone (Gilbert et al. 2010), where hypoxic and anoxic conditions are increasing in size, number, and frequency (Breitburg et al. 2018). Typically, coastal hypoxia and anoxia are recurrent seasonal phenomena owing to the seasonality of density stratification and algal growth (Diaz and Rosenberg 2008). In a fully oxygenated water column, methane concentrations are usually $< 0.05 \mu\text{M}$ (Reeburgh 2007), whereas the concentrations that accumulate under oxygen-deficient conditions can vary widely between systems, from 0.1 μM in the seasonally anoxic shelf waters of west India (Shirodkar et al. 2018) to 0.25 μM in the hypoxic Boknis Eck in the Baltic Sea (Steinle et al. 2017) and 1.9 μM in seasonally anoxic Saanich Inlet, British Columbia (Capelle et al. 2019), to reach 40 μM in the highly eutrophic and seasonally anoxic Chesapeake Bay on the US East coast (Gelesh et al. 2016). In these systems, methane is primarily sourced from anoxic sediments, where it is produced by methanogenic archaea (Ferry 1992). The spatiotemporal variability in methane dynamics contributes to shallow coastal waters being the most uncertain term in the marine methane budget (Weber et al. 2019) and highlights the importance of understanding how methane cycling is regulated on a seasonal scale and under different oxygen conditions. In particular, little is known about the efficiency of methane oxidation in the water column under different oxygen conditions, and how the process responds to the development of hypoxic and anoxic conditions and to the associated increase in methane concentrations.

*Correspondence: herdisgs@gmail.com

This is an open access article under the terms of the [Creative Commons Attribution-NonCommercial-NoDerivs](https://creativecommons.org/licenses/by-nc-nd/4.0/) License, which permits use and distribution in any medium, provided the original work is properly cited, the use is non-commercial and no modifications or adaptations are made.

Additional Supporting Information may be found in the online version of this article.

Author Contribution Statement: B.T., H.S., and L.B. designed experiments, carried out field work, and conducted experiments. S.M. carried out DNA extraction. Data were analyzed by C.S., H.S., and S.M. with support from B.T. and L.B. H.S. wrote manuscript assisted by B.T. and L.B., and all authors contributed to the final version of the manuscript.

In the presence of oxygen, methane is oxidized aerobically by methane-oxidizing bacteria using the oxygen-dependent particulate or soluble methane monooxygenases (for a review, see Trotsenko and Murrell 2008). Studies on pelagic methanotroph distributions are scarce, but members of the Gammaproteobacteria are suggested as important methane consumers in the ocean (Tavormina et al. 2010). Pelagic marine methanotrophs are capable of consuming methane to levels below atmospheric saturation concentrations (Reeburgh 2007) and thereby constitute an effective filter. Rates of aerobic methane oxidation from various marine water columns range several orders of magnitude (from 10^{-5} to 10^3 $\text{nmol L}^{-1} \text{d}^{-1}$; Mau et al. 2013), with much of the variability driven by differences in methane concentrations. Thus, the highest activities are measured in methane plumes (Steinle et al. 2015) and rates up to $150 \text{ nmol L}^{-1} \text{d}^{-1}$ are reported from hypoxic methane-enriched coastal waters (Steinle et al. 2017; Rogener et al. 2021).

Methane oxidation can also proceed anaerobically in anoxic waters. Anaerobic methane oxidation was first observed in marine sediments where it is coupled to the reduction of sulfate and has been studied extensively (Knittel and Boetius 2009). Since then, anaerobic methane oxidation has been shown to couple to the reduction of nitrate, nitrite, iron, and manganese (Ettwig et al. 2010; Haroon et al. 2013; Ettwig et al. 2016), and there is growing evidence that the process may be of importance in both marine and freshwater systems. Recently, nitrate- or nitrite-dependent anaerobic methane oxidation was proposed as a major pelagic methane sink in a marine oxygen minimum zone (OMZ; Thamdrup et al. 2019), and methane oxidation rates from anoxic depths in lakes have been proposed to be coupled to a variety of electron acceptors (van Grinsven et al. 2020; Roland et al. 2021). Still, the potential role of anaerobic methane oxidation in anoxic coastal waters remains to be explored.

Nitrate and nitrite are the most energetically favorable electron acceptors after oxygen and potentially relevant in coastal and freshwater systems, where they have become increasingly available as a result of eutrophication (Galloway et al. 2008). Methane oxidation coupled to nitrate reduction has been described for “*Candidatus Methanoperedens nitroreducens*” of the archaeal ANME-2d clade (new family *Methanoperedenaceae*, Haroon et al. 2013), members of which to date are primarily reported from freshwater sediments. Nitrite driven methane oxidation is mediated by bacteria of the candidate NC10 phylum, which are hypothesized to dismutate NO from nitrite reduction into N_2 and oxygen, the latter of which is used for intra-aerobic methane oxidation via the particulate methane monooxygenase pathway (Ettwig et al. 2010). Transcriptionally active “*Ca. Methylomirabilis oxyfera*” of the NC10 clade have been observed in OMZs (Padilla et al. 2016) and its relative “*Ca. Methylomirabilis limnetica*” was found to comprise up to 27% of the bacterial community in two anoxic lakes (Graf et al. 2018; Mayr et al. 2020), suggesting a major contribution to methane oxidation. Although considered to be obligate aerobes, gammaproteobacterial methanotrophs have also been shown to

thrive in various anoxic waters, such as in seasonally anoxic Saanich Inlet (Walsh et al. 2009; Torres-Beltrán et al. 2016), in anoxic lakes (Blees et al. 2014; Mayr et al. 2020), and in OMZs (Tavormina et al. 2013; Padilla et al. 2017). In some cases they may maintain their metabolism through in situ oxygen production by photosynthesis (Oswald et al. 2015). Yet members of the class are also capable of partial denitrification (Kits et al. 2015; Oswald et al. 2017; Padilla et al. 2017) and can oxidize methanol anaerobically (Dam et al. 2013). In Saanich Inlet, their depth distribution is highly suggestive of an involvement in anaerobic methane oxidation (Torres-Beltrán et al. 2016). Still, the metabolic ability for complete anaerobic methane oxidation has yet to be demonstrated.

In order to investigate how the seasonal development of water column stratification and anoxia influences methane oxidation and the methanotroph community in eutrophic coastal waters, we undertook monthly sampling during the development of anoxia in Mariager Fjord, Denmark. We combined biogeochemical measurements, experimental analysis of rates of aerobic and anaerobic methane oxidation, and analysis of the methanotrophic community through biomolecular analysis. Mariager Fjord is a brackish fjord on the northeastern coast of Jutland in Denmark, which due to nutrient loading from land combined with its topography has anoxic bottom waters between spring and late fall, but is typically flushed with oxygen-rich seawater during winter (Fig. S1; Fenchel et al. 1995; Fallesen et al. 2000). Mariager Fjord thus serves as a good model system for investigating how biogeochemical processes respond to the seasonal development of an oxic–anoxic interface.

Materials and methods

Sampling site

Water was sampled at Sta. NOR5503 (26-m water depth, $56^{\circ}3.76'N$, $009^{\circ}58.42'E$) in the central basin of Mariager Fjord, Denmark. Sampling was carried out together with the Danish Environmental Protection Agency, who recorded biweekly hydrographical profiles as a part of their long-term monitoring program in the fjord. The basin is redox stratified during most of the year as freshwater runoff from land maintains a stable halocline at mid-water depth that prevents oxygenation of bottom waters, and inflow of oxygen-rich seawater to the basin is limited by the long (> 20 km), narrow (< 2 km), and shallow (< 10 m) channel that connects the fjord with the Kattegat (Ramsing et al. 1996). However, nearly every winter a pulse of dense seawater enters the basin from the Kattegat and introduces oxygen to bottom waters (Fig. S1; Fenchel et al. 1995; Fallesen et al. 2000). The oxic water column typically persists for a few months before an oxic–anoxic interface appears again in the spring. The current seasonal study was conducted between April and October in 2019 after bottom waters had been oxygenated in January (Fig. 1).

Sample collection and chemical analysis

Hydrographic profiles were measured by the Danish Environmental Protection Agency approximately every other week

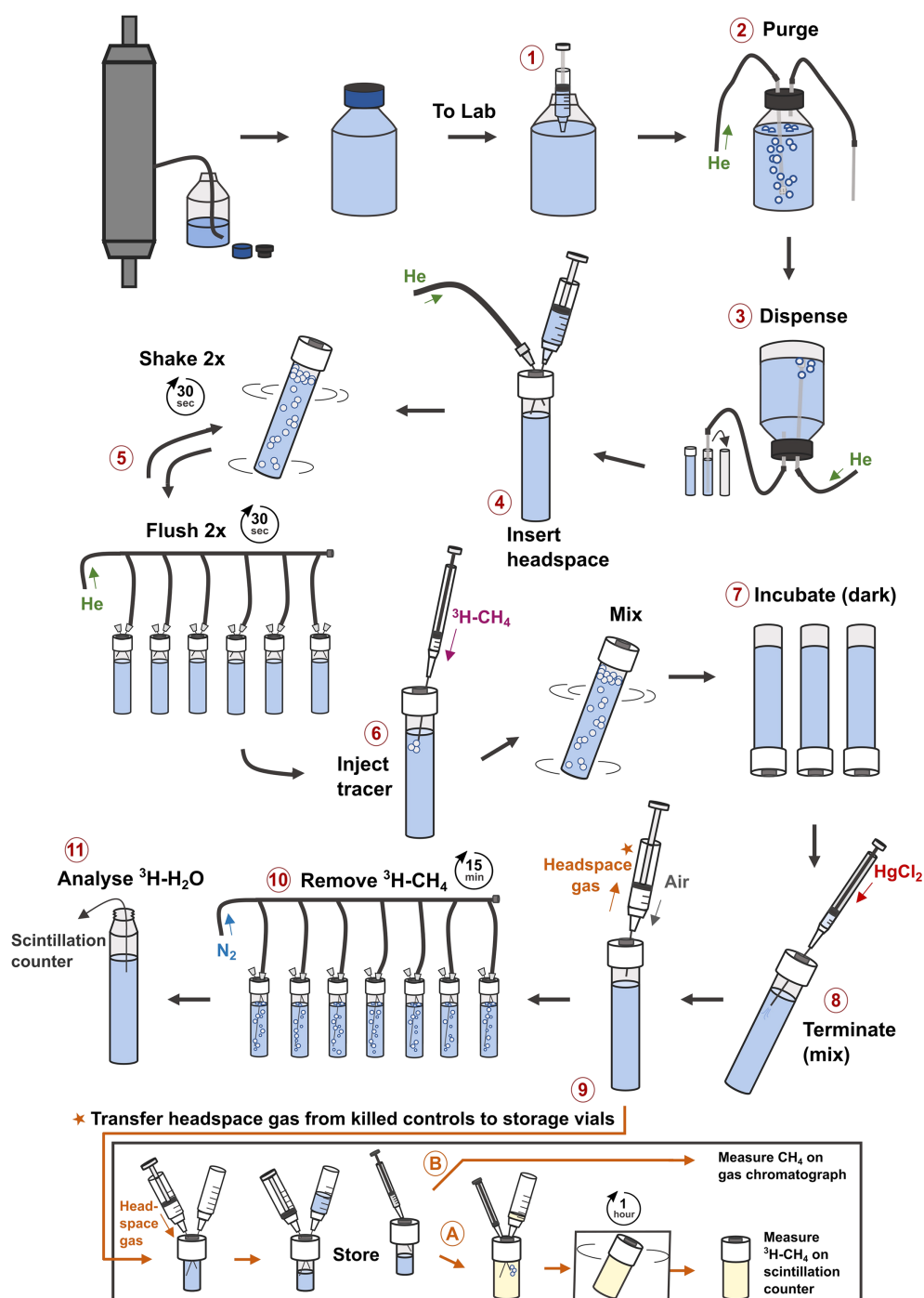


Fig. 1. A workflow schematic for incubation experiments. Water is sampled directly from a Niskin bottle through gas-tight viton tubing into a glass bottle (e.g., Schott Duran bottles) filled with overflow (> 2 volume changes) and sealed headspace free with a deoxygenated stopper. In the lab, (1) a headspace is introduced and (2) water is purged with He (30 min for a 500 mL glass bottle; flow rate 0.4 L min^{-1}) through a glass frit. (3) Reducing the He flow to approximately 0.1 L min^{-1} to control the flow rate, water is dispensed through glass and gas-tight viton tubing into 12 mL glass vials (Exetainer, Labco, UK) with overflow. (4) A 2 mL He headspace is introduced and then (5) the vial goes through 2 cycles composed of 30 s vigorous shaking and 30 s flushing with He (0.5 L min^{-1}). (6) $^3\text{H-CH}_4$ is injected (and CH_4 if needed) and mixed before (7) the vials are incubated in the dark at in situ temperature. (8) Microbial activity is terminated by injection of 100 μL saturated HgCl_2 and (9) 1 mL of headspace gas from killed controls is transferred to 3 mL storage vials pre-filled with degassed 0.5% wt vol^{-1} zinc chloride solution. The storage vial can be stored for days to weeks (e.g., until return to home laboratory) and is used to verify the addition of CH_4 and $^3\text{H-CH}_4$. (9A) headspace gas (20 μL) from the storage vial is transferred to a 6 mL Exetainer pre-filled with scintillation cocktail and 100 μL of air. Gas and liquid are equilibrated in the dark on a rocking table for 1 h before counting. (9B) CH_4 is measured by injection of the storage gas headspace (250 μL) into a gas chromatograph. (10) Remaining $^3\text{H-CH}_4$ is removed by 15 min of purging the water phase with N_2 (flow rate 0.4 L min^{-1} ; carried out within 1–2 h after termination of the final timepoint). (11) The activity of water ($^3\text{H-H}_2\text{O}$) is analyzed by scintillation counting of 4 mL aliquots.

between April and October using a CTD (conductivity, temperature, and depth-measuring device) equipped with an Aanderaa oxygen sensor 3830 (LOD 1 μM) and a PAR sensor (LI-COR LI-193). The data included here was downloaded from <https://odaforalle.au.dk/>. Profiles of biogeochemical and biomolecular parameters, and methane oxidation rates were sampled five times between May and October; on 02 May, 04 June, 30 July, 27 August, and 08 October 2019 (in subsequent presentation of these data, sampling dates will be referred to by month).

Water from discrete depths was collected with 5 L Niskin bottles and used to measure the concentrations of sulfide, methane, nitrate, nitrite, and ammonium, as well as for rate incubations and biomolecular analysis. Two Niskin bottles were fired simultaneously at the depths sampled for rates and biomolecular data, in order to have sufficient water for rate incubations and filtration of biomass. Concentrations of methane, nitrate and nitrite in the two bottles showed only minor differences, indicating that biogeochemical conditions in the two bottles were near identical (Figs. 3, 4F–J). All water was sampled through gas-tight viton tubing. Samples for sulfide were collected in 12 mL glass vials (Exetainers[®] Labco) filled from the bottom with three volumes overflow and no headspace. Samples were immediately amended with *N,N*-dimethyl-*p*-phenylenediamine reagent, stored in the dark and analyzed spectrophotometrically within 4 h of collection (Cline 1969). Water for methane analysis was sampled into 60 mL serum bottles with three volumes overflow. A 5 mL air headspace was inserted followed by 0.9 mL 6 N HCl for preservation and the bottle was crimp-sealed with a butyl rubber septum. Methane was analyzed the same day after samples had been shaken vigorously to equilibrate water and gas. Methane was determined by headspace analysis on a gas chromatograph (Thermo Trace 1300) equipped with an FID detector, and the concentration of methane was calculated using the temperature- and salinity-dependent distribution coefficient (Wiesenburg and Guinasso 1979). Samples for nitrite and nitrate were filtered through 0.2 μm cellulose acetate filters and analyzed spectrophotometrically using V^{3+} reduction and Griess reagent (García-Robledo et al. 2014). Nitrite was analyzed within 4 h of collection and samples for nitrate were stored dark at 4°C and analyzed the subsequent day. Samples for ammonium were collected in 12 mL Exetainers (samples from June to October were diluted 10–100 times in artificial seawater), amended with orthophthalaldehyde reagent and analyzed fluorometrically (Holmes et al. 1999).

Incubation experiments

Rates of methane oxidation were measured in batch incubations with $^3\text{H}\text{-CH}_4$ tracer (Valentine et al. 2001; Bussmann et al. 2015). The sampling and setup of incubations followed our laboratory's standard protocol developed to minimize oxygen contamination in shipboard incubations (initially applied to measure anaerobic rates in OMZ waters; Thamdrup et al. 2019). A workflow schematic of the protocol can be seen

in Fig. 1. The two Niskin bottles fired at each depth were mounted with gas-tight viton tubing and water was sampled simultaneously from the two Niskin bottles into 500 mL glass bottles with > 2 volumes overflow, such that equal amounts of water came from each Niskin bottle. Glass bottles were closed bubble-free with deoxygenated butyl rubber stoppers (De Brabandere et al. 2012). Samples were kept cool and dark until return to laboratory (< 4 h) where a headspace was introduced followed immediately by purging of the water for 30 min with He. Water was dispensed with ≥ 2 volumes overflow into 12 mL Exetainer vials that were immediately closed with deoxygenated chlorobutyl rubber septa. Each vial received a 2 mL He headspace before undergoing 2 cycles composed of 30 s of vigorous shaking followed by 30 s of flushing the headspace with He, to drive the remaining traces of oxygen out of the water.

In order to evaluate experimentally how the presence or absence of oxygen influenced methane oxidation we performed two timeseries incubations at each depth to measure rates of (1) anaerobic methane oxidation and (2) aerobic methane oxidation. The set of vials intended for analysis of aerobic methane oxidation were injected with oxygen (as 100% pure oxygen gas, between Steps 5 and 6 in Fig. 1) to a target concentration of 30 μM . Since the purging of samples that accompanies the setup of incubations removes the ambient methane pool, all vials received unlabeled methane (injected as methane-saturated water) to re-establish the in situ methane concentration. Injection volumes were determined based on the distribution coefficient (Wiesenburg and Guinasso 1979). Each vial was then injected with tracer as 10 μL of $^3\text{H}\text{-CH}_4/\text{N}_2$ tracer mixture. The tracer mixture was prepared in February 2019 from a 20 Ci mmol^{-1} single labeled $^3\text{H}\text{-CH}_4$ aliquot (American Radiolabeled Chemicals). The aliquot contained 1 mCi in ~ 10 mL and was diluted with N_2 to a final activity of ~ 0.05 mCi mL^{-1} in the tracer mixture. The mixture was stored in a Hungate tube over NaCl-saturated water until 2–4 d before each experiment, when a fraction of tracer mixture was transferred through two Exetainers prefilled with 50% wt vol^{-1} NaOH (for cleaning). In each transfer step, the Exetainer containing tracer mixture and NaOH was shaken vigorously for 30 s. The mixture was finally stored over alkaline ascorbate as an oxygen scrubber (Thamdrup et al. 2019), until it was injected into incubations. Incubations were initiated within 10 h of sample collection, took place in the dark at near in situ temperature, and were terminated in duplicates at four timepoints; 0 (killed controls), 6, 12, and 24 h, by injection of 100 μL saturated HgCl_2 . Terminated samples were stored under the same conditions as live incubations during the 24-h incubation period. The aqueous concentration of oxygen in incubations was monitored during the incubation (see “Monitoring oxygen in incubations”).

After termination of the final timepoint (24 h), 1 mL of headspace gas was transferred from killed controls to storage vials (3 mL Exetainers) prefilled with a degassed 0.5% wt vol^{-1}

zinc chloride solution. The storage vials (containing gas from killed controls) were kept at 21°C until analysis, where they served to quantify the addition of unlabeled methane and tracer to incubations (details below). Within 1–2 h after termination of the final timepoint, incubation vials were purged for 15 min with N₂ bubbling through the water phase (flowrate 0.4 L min⁻¹) to remove all ³H-CH₄ from the sample. The activity of ³H in water ($A_{\text{H}_2\text{O}}$) was then measured by scintillation counting of 4 mL of sample within 12–18 h after termination of the final timepoint. Analysis of ³H-CH₄ in the storage vials was carried out 1–4 d after termination of each experiment following Thamdrup et al. (2019). The concentration of unlabeled methane in incubations was determined from the remaining gas in the storage vial by injecting 250 μL of the headspace gas into a gas chromatograph.

$A_{\text{H}_2\text{O}}$ increased approximately linearly with incubation time (no time lag) and rate constants, k , were calculated from the slope of the linear regression of $A_{\text{H}_2\text{O}}$ plotted over time, by $k = A_{\text{H}_2\text{O}} \times t^{-1} \times A_{\text{CH}_4}^{-1}$. Since incubations were carried out with in situ concentrations of methane (Fig. S5), we calculated the rates of methane oxidation as the product of k and the in situ concentration of methane ($k \times [\text{CH}_4]_{\text{in situ}}$; Reeburgh et al. 1991; Valentine et al. 2001). Rates were integrated over the 4–5-m depth interval analyzed for rates, using the trapezoidal rule. A t -test determined whether rates were significantly different from zero and a two-sample t -test was used to determine if rates in incubations injected with oxygen were significantly different from rates in incubations not injected with oxygen.

Abiotic transfer of ³H between the ³H-CH₄ tracer and water is a well-known phenomenon with the rate of transfer depending on the matrix (Bussmann et al. 2015). To our knowledge, only one study has previously reported using the ³H-CH₄ tracer to measure rates of methane oxidation in sulfidic waters, but abiotic transfer was not investigated (Reeburgh et al. 1991). To investigate the potential for abiotic transfer of activity between ³H-CH₄ and water in our incubations and evaluate the validity of the ³H-CH₄ method in sulfidic waters, we undertook a sampling on 21 October 2019 for a tracer assessment experiment at three depths spanning a gradient in in situ sulfide concentration of 0–32 μM. This in situ concentration range corresponded approximately to the range of 0–38 μM encountered across the 19 samples collected for methane oxidation rate determinations, of which 7 contained detectable sulfide (LOD 1 μM). The purging of samples during incubation setup (Step 2 in Fig. 1) was shown to remove approximately two-thirds of the ambient sulfide pool in agreement with a previous report (Jensen et al. 2009). Thus, the tracer assessment experiment covered experimental sulfide concentrations of 0–10 μM, while two incubation experiments (18 m in August and 19 m October, marked with asterisk in Fig. 4) contained substantial sulfide (between 7 and 14 μM).

The incubation setup for the tracer assessment experiment was identical to that used in the anoxic seasonal experiments (details in Supporting Information Methods and Discussion).

This assessment showed that sterile filtered incubations with 10 μM sulfide had an abiotic rate that was 11% of the methane oxidation rate measured in parallel standard practice incubations. Similarly, killed control incubations exhibited transfer rates ≤ 12.5% of the standard practice rate at the same depth (details in Supporting Information Methods and Discussion), implicating overall a minor effect on the calculated methane oxidation rates.

Rates of denitrification were determined alongside methane oxidation rates following the method outlined in (De Brabandere et al. 2014). For this purpose, an additional 500 mL glass bottle was filled at each depth. In the laboratory, the bottle was amended with ¹⁵N-labeled nitrite (to 25 μM) before undergoing the same downstream treatment as previously described for methane oxidation rates, to minimize oxygen contamination in incubations. Incubations were injected with unlabeled methane as methane-saturated water to match the in situ concentration and were carried out under the same conditions as described previously. The production of ¹⁴N¹⁵N and ¹⁵N¹⁵N was analyzed on a gas chromatography-isotope ratio mass spectrometer (GC-IRMS; custom made GC setup coupled to a Thermo Delta V Plus mass spectrometer; Dalsgaard et al. 2012). Rates were obtained from the regression slopes of ¹⁴N¹⁵N and ¹⁵N¹⁵N accumulation over time and the mole fraction of ¹⁵N in the initial substrate pool according to (Thamdrup and Dalsgaard 2002). A t -test determined whether rates were significantly different from zero.

Monitoring oxygen in incubations

The aqueous oxygen concentration was monitored during the incubations in a subset of vials mounted with either full range optode spots (OXSP5 Pyroscience GmbH, vials injected with oxygen) or trace range optode spots (TROXSP5 Pyroscience GmbH, vials not injected with oxygen). Oxygen was logged every 6 h during incubation time using a Firesting fiber-optic oxygen meter (Pyroscience GmbH). The factory calibration of spots was corrected for the zero-reading obtained by addition of sodium dithionite at the end of each experiment. The concentration of oxygen in the incubations injected with oxygen was $28 \pm 2.5 \mu\text{M}$ and did not decrease by more than 5 μM during the 24-h incubations, while the concentrations of oxygen in vials not injected with oxygen was below the detection limit of the method (< 50 nM). For simplicity, in the following presentation of data, these two experimental conditions will be referred to as oxic (~ 28 μM oxygen) and anoxic (< 50 nM oxygen).

DNA sampling, extraction, and analysis

Biomass for analysis of biomolecular parameters (amplicon sequencing of bacterial 16S rRNA and PCR targeting 16S rRNA of archaea) was collected and extracted following the protocol described in (Padilla et al. 2016; see Supporting Information Methods for details).

Long-length bacterial 16S rRNA gene amplicons were synthesized from a subset of samples at the Next Generation Sequencing Facility of the Vienna Biocenter (www.vbcf.ac.at) using the bacteria-specific primers 27F (5'-AGRGTTYGATY-MTGGCTCAG-3') and 1492R (5'-RGYTACCTTGTTACGACTT-3'). Barcodes were added in a second round of amplification with PacBio Barcoded Universal primers and multiplexed onto two SMRT cells prior to sequencing on two separate runs on a PacBio Sequel. The resulting data was analyzed with PacBio tools (<https://github.com/PacificBiosciences/pbbioconda>), with pbccs for producing circular consensus sequences, lima for demultiplexing, and fastq2bam for converting the data to fastq files. We subsequently trimmed all nonbiological nucleotides from the data and inferred amplicon sequencing variants (ASVs) using dada2 (Callahan et al. 2016) in the RStudio software environment. Both sequencing runs were merged with the “mergeSequenceTables” commands before the de-novo Chimera removal of the dada2 workflow. We used the RDP classifier of the dada2 package to taxonomically classify ASVs using the SILVA v138 database as a reference. Relative abundances were calculated as the fraction of ASV counts and total sample count. ASVs representing putative methanotrophic taxa were identified by inspection of the taxonomic annotations using keyword searches and manual parsing.

MUSCLE (Edgar 2004) was used to align the 16S rRNA gene sequences representing identified methanotrophs from Mariager Fjord with 16S rRNA gene sequences of methanotroph isolates in (Knief 2015), closely related environmental sequences obtained via BLASTN, and a selection of published environmental methanotroph sequences (Walsh et al. 2009; Tavormina et al. 2013; Mayr et al. 2020). A phylogenetic tree was constructed using IQTree v. 2.1.2 (Minh et al. 2020). The model finder selected TN + F + R3 as the best fit substitution model (Kalyaanamoorthy et al. 2017) and branch support was calculated via 1000 nonparametric bootstrap replicates. Sequence data has been submitted to the Short Read Archive at NCBI under the accession number: PRJNA749906.

As archaea are not targeted by the primers used for 16S rRNA amplicon analysis, we applied a PCR analysis to screen for anaerobic methane-oxidizing archaea (ANME). For this we used the 16S rRNA targeting primer sets: A349F and 519R for archaea (Ovreås et al. 1997; Takai and Horikoshi 2000), ANME2a-426F and 1242R for ANME-2a, ANME2b-402F and 1251R for ANME-2b (Miyashita et al. 2009), 2cF and R for ANME-2c (Vigneron et al. 2013) and AAA641F and 834R for ANME-2d (Schubert et al. 2011; Vaksmaa et al. 2017). The PCR reactions were performed in duplicates on a Bio-Rad (CFX Connect, Real-Time System; see Supporting Information Methods for PCR conditions).

To further constrain the abundance of ANME-2d, we carried out a quantitative PCR analysis of Archaea and ANME-2d. Amplicons of the expected product size were detected by gel electrophoresis and cloned using the Invitrogen™ TOPO™ TA Cloning Kit, according to manufacturer instructions. Gene

copy numbers of Archaea and ANME-2d were obtained using the primer pairs A349F/519R (Ovreås et al. 1997; Takai and Horikoshi 2000) and AAA641F/834R (Schubert et al. 2011; Vaksmaa et al. 2017), respectively (see Supporting Information Methods for qPCR conditions).

Flux calculations

The vertical flux of methane due to eddy diffusion was estimated by multiplying the concentration gradient with the vertical turbulent mixing coefficient:

$$F_z = -K_z \frac{dC}{dz} \quad (1)$$

where F_z is the vertical flux, dC/dz is the concentration gradient of methane, and K_z is the mixing coefficient. For each month, values for K_z were calculated from the density gradient $d\rho/dz$ obtained from CTD measurements (Lewis and Landing 1991):

$$K_z = a_0 \left(-\frac{g}{\rho_z} \frac{d\rho}{dz} \right)^{-0.5} \quad (2)$$

where g is the gravitational constant, ρ_z is the density at depth z , and a_0 is a system specific constant representing the internal wave energy. We used an a_0 of $0.0005 \text{ cm}^2 \text{ s}^{-2}$ as estimated previously for Mariager Fjord (Zopfi et al. 2001; Jensen et al. 2009). Calculations are based on the assumption that a_0 is constant over time.

Results

Seasonality of stratification

The biweekly CTD measurements performed in Mariager Fjord between April and October 2019 showed a persistent halocline at 12–16-m depth (Fig. 2A). Temperature profiles revealed an expected temperature distribution for a shallow temperate water column (Fig. 2B), where water temperature was near uniform at $\sim 7^\circ\text{C}$ in April, before a thermocline appeared in early May, coinciding with the halocline at 15-m depth. The thermocline gradually migrated deeper and strengthened as surface waters warmed to $\sim 20^\circ\text{C}$ over summer, before relaxing again in the fall as surface waters cooled to 13°C in October. Oxygen measurements demonstrated a seasonal progression in redox stratification that is typical for the fjord (Figs. 2C, S1). The basin had been flushed with oxygen-rich water in January of 2019 (Fig. S1), and oxygen reached the sediment–water interface (26 m) until late May, when an oxic–anoxic interface appeared close to the sediment–water interface (Fig. 2C; based on a CTD oxygen detection limit of $1 \mu\text{M}$). The interface shoaled to reach $\sim 13 \text{ m}$ in August, before deepening to 17–18 m in the fall (Fig. 2C). The oxygen gradient toward the oxic–anoxic interface became steeper over the course of the study, with oxygen

decreasing from $50 \mu\text{M}$ to below detection over a depth range of approximately 5 m in May and June, compared to 1–2 m in August and October. In late August salinity and oxygen profiles indicated an intrusion at $\sim 15\text{-m}$ depth of more saline water containing $\sim 50 \mu\text{M}$ oxygen (Figs. 2, 3D). Light penetrated to maximally 12 m in spring and to $< 7\text{-m}$ depth between June and October (Fig. S2; $> 1\%$ of incident light).

Profiles of biogeochemical parameters were sampled at 4–8-week intervals between 02 May and 08 October 2019 (Figs. 3, S3). The seasonal progression in oxygen conditions was reflected in concentration profiles of nitrate and nitrite (Fig. 3F–J). In the entirely oxic water column in May, nitrate ranged between 40 and $60 \mu\text{M}$ at all investigated depths while nitrite was only observed between 10 and 15 m ($\sim 1 \mu\text{M}$). The onset of anoxia in June initiated a drawdown of nitrate in the bottom water with a consequent accumulation of $6 \mu\text{M}$ nitrite at anoxic depths (24–25 m). In July, nitrate and nitrite were depleted 2–4 m below the oxic–anoxic interface with up to $8 \mu\text{M}$ nitrate and $3 \mu\text{M}$ nitrite found at anoxic depths, whereas in August nitrate and nitrite were nearly depleted at the same depth as oxygen. Sulfide was never detected at oxic depths but accumulated below the oxic–anoxic interface with the highest levels seen at 24 m near the sediment–water interface in July and August (77 and $88 \mu\text{M}$, respectively). In October the oxic–anoxic interface had shifted slightly downward (to 17.5 m) and although nitrate was still depleted near the oxic–anoxic interface, the concentration of nitrite peaked at 16-m depth ($14 \mu\text{M}$) and remained $> 0.6 \mu\text{M}$ at all anoxic depths. That

same month the maximum concentration of sulfide had dropped to $\leq 52 \mu\text{M}$. Ammonium was $\leq 1.5 \mu\text{M}$ at all depths in May but steadily increased below the oxic–anoxic interface from June until October, where it reached $75 \mu\text{M}$ at 24-m depth (Fig. S4). Above the interface, ammonium ranged between 4 and $35 \mu\text{M}$.

Methane accumulated immediately when bottom waters of Mariager Fjord became anoxic (Fig. 3A–E). At oxic depths, the concentration of methane was $< 0.1 \mu\text{M}$ across all months, and between June and October there was a pronounced methane minimum in the oxycline just above the oxic–anoxic interface. The concentration of methane below the interface grew steadily from $0.23 \mu\text{M}$ in June to peak at $1.4 \mu\text{M}$ at 24-m depth in August. The spatiotemporal distribution of methane at anoxic depths was similar to that of sulfide, with methane concentrations being about 50-fold lower. Methane concentrations increased linearly with depth below the oxic–anoxic interface, except in October, where they stabilized at $\sim 1 \mu\text{M}$ below 19-m depth. Similar to the trend seen in oxygen profiles, the gradient of methane toward the oxic–anoxic interface steepened over the course of the study.

Rate constants and rates of methane oxidation

Rate constants (k) and rates of methane oxidation were measured once a month at three to four depths spanning the oxic–anoxic interface, except in May, when the oxic–anoxic interface was absent and rate incubations spanned a gradient in ambient oxygen concentration of 30– $120 \mu\text{M}$ (Fig. 3A–E). For each depth we conducted two sets of incubations that we refer to as oxic ($\sim 28 \mu\text{M}$ oxygen) and anoxic ($< 50 \text{ nM}$ oxygen). In all incubations, the ^3H activity in the water increased approximately linearly during the 24 h of incubation time with no apparent time lag.

Overall, rate constants of methane oxidation in Mariager Fjord ranged between $0.09\text{--}0.8 \text{ d}^{-1}$ (Fig. 4A–E). In most samples (15 out of 19), there was no significant difference ($p > 0.05$) between methane oxidation activity in oxic and anoxic incubations. However, rate constants measured from the shallowest depth in May and above the oxic–anoxic interface in June (three depths in total) were lower (35–50%) in anoxic compared to oxic incubations, while the activity at one depth below the interface in August (17 m) was 33% higher in the anoxic incubation. In general, rate constants of methane oxidation did not change markedly with depth across the oxic–anoxic interface, except in August, where k in both oxic and anoxic incubations increased from $0.2\text{--}0.3 \text{ d}^{-1}$ above the interface to $0.6\text{--}0.8 \text{ d}^{-1}$ below. Instead, the activity increased during the study period as the stratification developed over the summer. In May and June, when the oxic–anoxic interface was either absent (May) or had just emerged near the sediments (at 24 m, June), rate constants were $0.09\text{--}0.33 \text{ d}^{-1}$, with the highest activities occurring close to the sediment–water interface in June. Rate constants did not increase notably between June and July ($0.16\text{--}0.33 \text{ d}^{-1}$), after

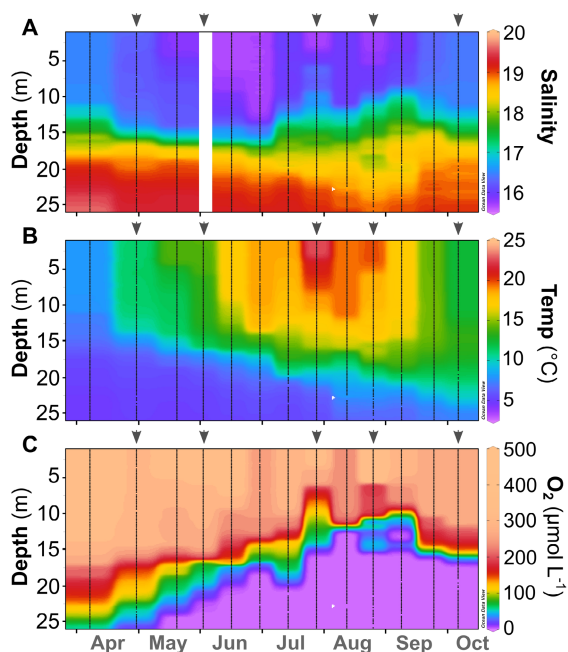


Fig. 2. Seasonal dynamics of salinity (A), temperature (B), and oxygen (C) between April and October 2019 in Mariager Fjord. Arrows show dates of sampling for biogeochemical and biomolecular parameters. Salinity data was not available from June 4.

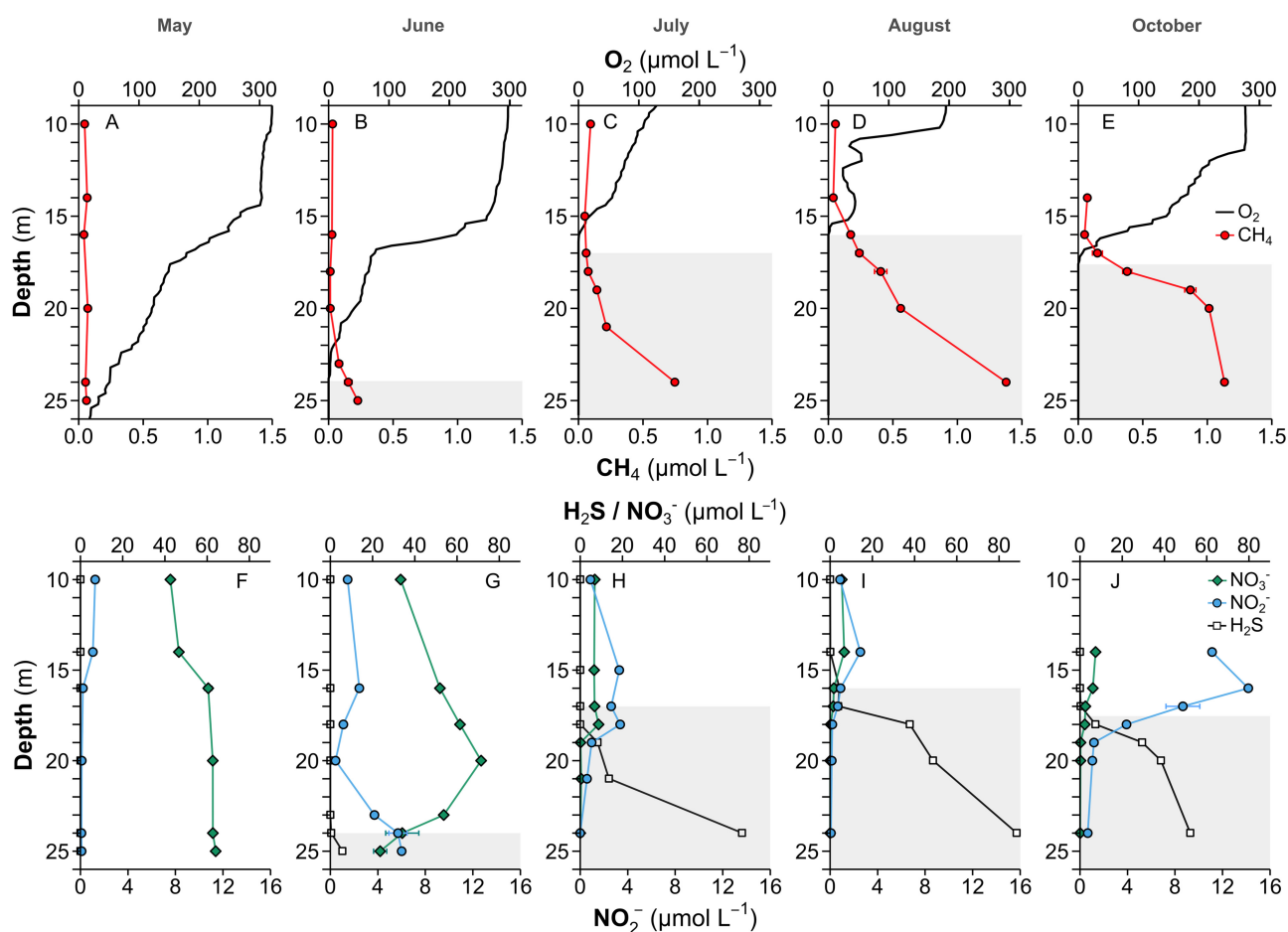


Fig. 3. Depth profiles of oxygen and methane (A–E), and nitrate, nitrite, and sulfide concentrations (F–J) between May and October, 2019 in Mariager Fjord. Samples were collected on 02 May (A,F), 04 June (B,G), 30 July (C,H), 27 August (D,I), and 08 October (E,J) 2019. Data collected at 10 m water depth and below is shown (full depth profiles are shown in Supporting Information Fig. S3), the sediment–water interface is located at 26 m and the shaded area indicates anoxic depths ($< 1 \mu\text{M}$ oxygen). Error bars on profiles of methane, nitrate, and nitrite concentrations show the range in concentration between two Niskin bottles fired simultaneously at each depth sampled for methane oxidation rates (3–4 depths near the oxic–anoxic interface). Depth profiles of ammonium concentrations are shown in Supporting Information Fig. S4.

the oxic–anoxic interface had shoaled to 17 m, but activities became markedly higher in August ($0.2\text{--}0.8 \text{ d}^{-1}$), especially at depths below the interface. The activity remained high in October ($0.3\text{--}0.4 \text{ d}^{-1}$) and was uniform across investigated depths (16–19 m). Incubations from the deepest depths analyzed for methane oxidation rates in August and October contained $7\text{--}10 \mu\text{M}$ sulfide (Fig. 4D,E; marked with asterisk).

Incubations were carried out with near in situ concentrations of methane (e.g., Fig. S5), and rates of methane oxidation could therefore be obtained by multiplying rate constants (Fig. 4A–E) with the in situ methane concentration (Fig. 3A–E). Since rate constants did not vary greatly with depth, rates were primarily determined by the concentration of methane and increased linearly with depth in months where methane accumulated in anoxic bottom waters (Fig. S6A–E, only anoxic incubations shown). Only rates from anoxic incubations are presented, since the difference between oxic and anoxic incubations was minimal (Fig. 4D,E, insignificant, $p > 0.05$, in 15 of the 19 samples).

In the oxic water column in May rates were $0.007\text{--}0.008 \mu\text{mol L}^{-1} \text{ d}^{-1}$ but increased as bottom waters became anoxic in June and July reaching $0.016\text{--}0.063 \mu\text{mol L}^{-1} \text{ d}^{-1}$ below the oxic–anoxic interface. Rates further increased as the methane gradient became steeper over summer and fall. The highest rates were measured below the oxic–anoxic interface in August and October, reaching 0.22 and $0.37 \mu\text{mol L}^{-1} \text{ d}^{-1}$, respectively. Rates of denitrification were measured in incubations with in situ concentrations of methane. Denitrification was detected at all anoxic depths at rates ranging from 0.2 to $7.7 \mu\text{mol N}_2 \text{ L}^{-1} \text{ d}^{-1}$, whereas no denitrification was detected at any depth in May nor at 16-m depth in October (Fig. S6F–J).

The methanotroph community

Sequencing of full length 16S rRNA gene amplicons found methanotroph-related sequences at all depths examined in Mariager Fjord (no sequence data were available for July). We identified three methanotroph affiliated ASVs (ASV 10, ASV

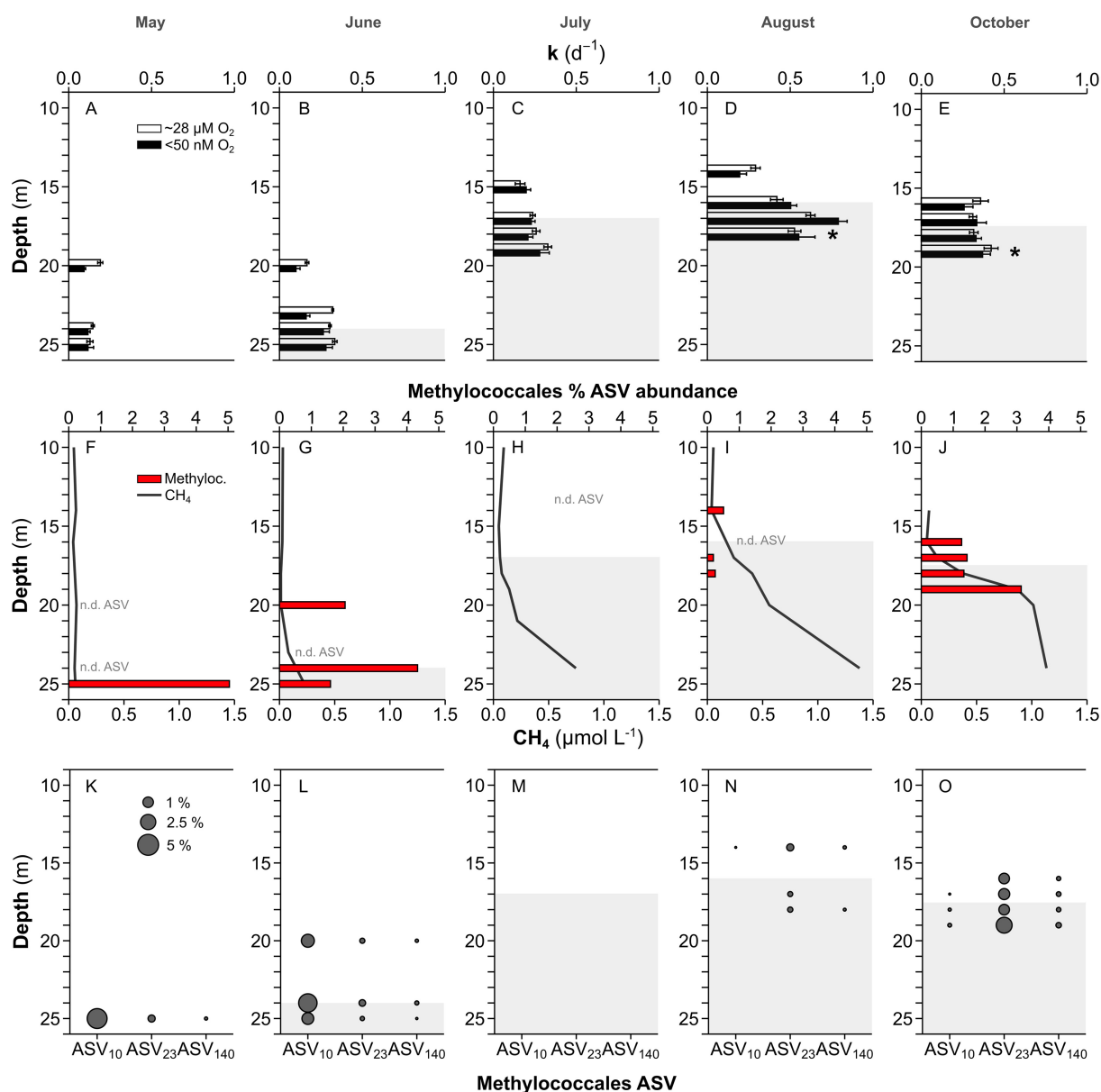


Fig. 4. Depth distribution of methane oxidation rate constants (k ; **A–E**) measured in incubations with $\sim 28 \mu M$ oxygen (white) or < 50 nM oxygen (black), relative abundance of Methylococcales and methane concentrations (**F–J**), and the contribution of individual Methylococcales ASVs to the total population (shown as percent of total ASVs; **K–O**) between May and October, 2019, in Mariager Fjord. Samples were collected on 02 May (**A, F, K**), 04 June (**B, G, L**), 30 July (**C, H, M**), 27 August (**D, I, N**), and 08 October (**E, J, O**) in 2019. Data shown for the depth range 10–25 m where the base of the graph (26 m) marks the sediment–water interface and the shaded area indicates anoxic depths ($< 1 \mu M$ oxygen). Error bars on rate constants (**A–E**) represent standard error. Asterisks (on **D–E**) show depths where sulfide concentrations in < 50 nM oxygen incubations were $7–14 \mu M$ (see Supporting Information Methods and Discussion). No ASV data was available in July, or from 20 and 24 m in May, 23 m in June, or at 16 m in August (n.d. ASV).

23, and ASV 140), which all belonged to the gammaproteobacterial order Methylococcales. We did not detect any anaerobic methane oxidizers related to “*Ca. Methyloirabilis oxyfera*” (Ettwig et al. 2010) with the PacBio bacteria-specific primers and no ANME archaea were detected by the PCR analysis. In addition, ANME-2d abundances were shown to be below detection by qPCR (< 100 ANME-2d 16S rRNA gene

copies mL^{-1} ; Fig. S7). The relative abundance of Methylococcales in Mariager Fjord ranged between 0.2% and 5% of total amplicons at all investigated depths, the highest abundance occurring in May and the lowest in August (Fig. 4F–J). There was no clear structure in Methylococcales abundances with respect to the oxic–anoxic interface between months.

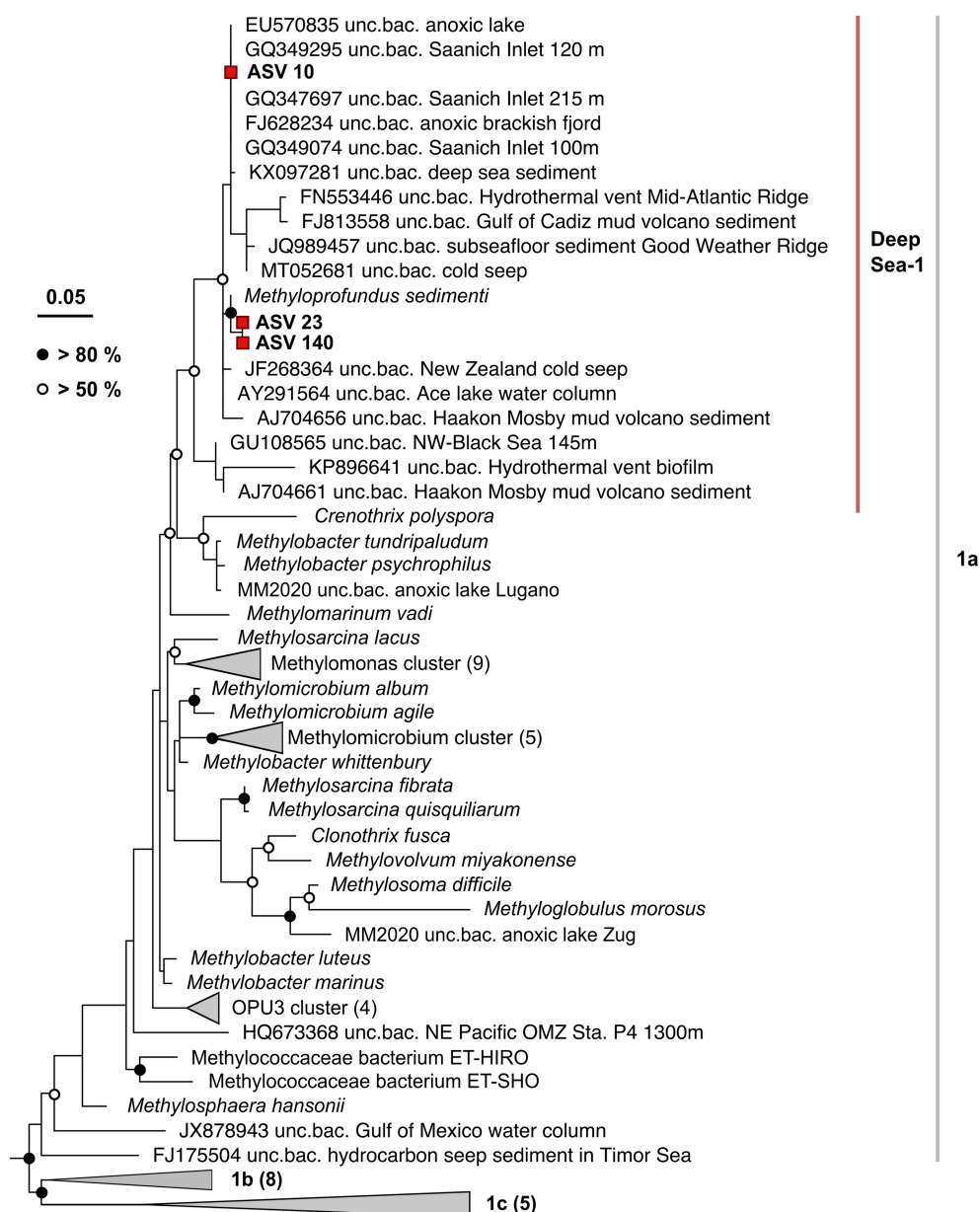


Fig. 5. Maximum likelihood phylogeny of near full length 16S rRNA gene sequences of gammaproteobacterial methanotrophs in Mariager Fjord. The scale bar denotes nucleotide substitutions. Bootstrap values > 80% (black circles) and > 50% (white circles) are shown (1000 maximum likelihood replicates). Strain sequences are adopted from Knief (2015) and MM2020 lake sequences are from Mayr et al. (2020). The red line indicates the Deep Sea-1 clade of the Methylococcales order.

Examining the individual Methylococcales ASVs we observed differences in their proportional abundance and temporal distribution (Fig. 4K–O). At each sampling, the methanotroph community was dominated by a single ASV which constituted 85–100% of the total methanotroph sequences at any investigated depth, independent of redox conditions. The dominating ASV, however, shifted from ASV 10 in May and June to ASV 23 in August and October. The relative abundance of ASV 140 remained < 15% of methanotroph

sequences across all months sampled. Phylogenetic analysis of the three ASVs classified them as members of the Deep Sea-1 clade (Fig. 5), which contains the genus *Methyloprofundus sedimenti* (Tavormina et al. 2015).

Discussion

By following the onset of anoxia in Mariager Fjord, our study provided the opportunity to investigate the roles of

aerobic and anaerobic methane oxidation in methane removal during the gradual development of redox stratification over summer. We evaluate the efficiency of the observed microbial methane filter in mitigating the release of methane to surface waters and thus, ultimately, preventing the accumulating methane pool from contributing to increased emissions to the atmosphere.

Development of seasonal anoxia and steep concentration gradients

There was a clear seasonal progression in the redox stratification in Mariager Fjord in 2019, where the onset of anoxia in May preceded the development of steep redox gradients over summer and early fall (Fig. 2C). Oxygen concentrations followed the typical pattern observed in previous studies in Mariager Fjord (Fenchel et al. 1995; Fallesen et al. 2000) and in the long-term monitoring program carried out by the Danish Environmental Protection Agency (Fig. S1). However, compared to conditions in the 20th century, when oxygenation events only occurred every 1–3 years (Fenchel et al. 1995; Ramsing et al. 1996; Fallesen et al. 2000), the winter oxygenation events now seem more regular, since bottom waters were oxygenated every winter between 2011 and 2020, except in 2013 (Fig. S1). Thus, in its present state, Mariager Fjord can be used as a model system for studying seasonal anoxia, with results that are relevant to various other coastal seasonally anoxic systems such as the Indian continental shelf (Shirodkar et al. 2018), estuaries like Chesapeake Bay (Gelesh et al. 2016), and fjords such as Saanich Inlet (Torres-Beltrán et al. 2017; Capelle et al. 2019), as well as seasonally anoxic lakes that undergo a similar gradual development of redox gradients during their post-turnover phase (e.g., Diao et al. 2017).

The gradual steepening of redox gradients over summer and fall implies increasing fluxes of oxidized and reduced substrates toward the oxic–anoxic interface, since the specific density gradient across the interface weakened over the same time period ($d\rho/dz$ from 0.37 to 0.29 kg m⁻³ m⁻¹ between July and October, based on a 6-m depth interval transecting the oxic–anoxic interface; no salinity data available from June). A higher substrate flux typically sustains a larger microbial community capable of efficient substrate conversions (Brune et al. 2000). However, in a seasonally anoxic system, where redox gradients develop gradually, the generation time of the microbial populations near the oxic–anoxic interface may potentially determine how rates respond to the accumulation of substrate. Generation times of methanotrophs in culture vary considerably, from hours or days in some aerobic gammaproteobacterial methanotrophs (Graham et al. 1993; Hirayama et al. 2013) to > 2 months for some anaerobic methane oxidizers (Knittel and Boetius 2009). Thus, if the growth rate of methanotrophs in the water column is slow, the accumulation of methane in anoxic bottom waters could result in an increased turbulent-diffusive flux across the oxic–anoxic

interface, or, if growth rates of methanotroph populations near the oxic–anoxic interface are high enough, they may continuously mitigate the release of methane from bottom waters.

In Mariager Fjord, methane accumulated in the bottom water from < 0.1 μM in May to the maximum of 1.4 μM in August (Fig. 3A–E). A study performed there in August 1994, when bottom waters had remained anoxic since winter 1992–1993, measured 40 μM methane near the sediment–water interface (Fenchel et al. 1995), suggesting that methane may continue to accumulate if not interrupted by an oxygenation event. The rate of methane accumulation over time was similar to that seen in seasonally anoxic Saanich Inlet where concentrations typically increase from $\sim 0.05 \mu\text{M}$ in winter to $\sim 1.3 \mu\text{M}$ during summer (Capelle et al. 2019). However, since the anoxic water column in Mariager Fjord is about 10 times shallower than in Saanich Inlet ($\sim 10 \text{ m}$ and $\sim 100 \text{ m}$, respectively) the methane gradient in Mariager is steeper and the resulting flux correspondingly higher.

The increase in methane concentrations with depth in Mariager Fjord is indicative of a sediment source. Indeed, Fenchel et al. (1995) estimated the methane efflux from anoxic sediments in Mariager Fjord to be 0.3–1.5 mmol m⁻² d⁻¹. These values are in line with fluxes reported from other highly eutrophic coastal sediments, such as seasonally hypoxic Randers Fjord (up to 0.4 mmol m⁻² d⁻¹; Abril and Iversen 2002) and saline Lake Grevelingen (0.6–2.2 mmol m⁻² d⁻¹; Egger et al. 2016). In these environments it is expected that rapid sedimentation rates sustain the high methane fluxes, by providing abundant substrate for methanogenesis in surface sediments, as well as reducing the residence time of slow-growing anaerobic methanotrophs in the sulfate–methane transition zone (Egger et al. 2016), emphasizing the importance of understanding the methane-oxidizing capacity of the overlying water column.

Efficient methane oxidation across an emerging redox boundary mediated by Methylococcales

With the aim of investigating the seasonal dynamics of aerobic and anaerobic methane oxidation, we carried out two parallel sets of incubations with $\sim 28 \mu\text{M}$ oxygen and < 50 nM oxygen, respectively (Figs. 4A–E, S6A–E). Several lines of evidence suggest that methane oxidation in incubations with < 50 nM oxygen occurred anaerobically. First, rates of methane oxidation in incubations from multiple depths (e.g., all anoxic depths in June, August, and October) were > 50 nmol L⁻¹ d⁻¹. This is higher than what could have been sustained by the maximum possible oxygen concentration in the incubations, despite applying the conservative 1 : 1 oxygen to methane consumption ratio of carbon assimilating aerobic methanotrophs, as typically the ratio is closer to 2 : 1 (Naguib 1976). In addition, a system with high primary production like Mariager Fjord (Fallesen et al. 2000) will harbor an abundant heterotrophic community (Andersen and

Sørensen 1986) and the methanotrophs would therefore face strong competition for the limited oxygen pool from oxygen-respiring heterotrophs. A previous study in Mariager Fjord estimated oxygen consumption rates of $3.4 \mu\text{M d}^{-1}$ just above the oxic–anoxic interface (Ramsing et al. 1996), which is in line with the oxygen drawdown of up to $5 \mu\text{M d}^{-1}$ evident in our oxic incubations. These rates would deplete an oxygen pool of $< 50 \text{ nM}$ in less than 10 h, assuming half-saturation (K_m) values in the 66–259 nM range as estimated for various Danish coastal waters (Tiano et al. 2014). Incubations would thus be functionally anoxic for most of the 24 h incubation time. Since methane oxidation rates were linear over the full 24 h incubation time, there was no indication of a shift from aerobic to anaerobic metabolism. We also exclude photosynthesis as an internal oxygen source as incubations were carried out in the dark. We thus conclude that the methane oxidation activity observed in the incubations with $< 50 \text{ nM}$ oxygen was anaerobic. Therefore, in subsequent discussion, we refer to the two incubation types as oxic and anoxic and will henceforth refer to the activity observed in each of the incubations as aerobic and anaerobic methane oxidation, respectively.

Overall, rate constants of methane oxidation in Mariager Fjord ($0.09\text{--}0.8 \text{ d}^{-1}$, Fig. 4A–E) correspond to the upper range of rate constants reported from hypoxic coastal waters ($\leq 0.4 \text{ d}^{-1}$, Rogener et al. 2021; $\leq 0.084 \text{ d}^{-1}$, Steinle et al. 2017) and they agree well with values seen below the oxic–anoxic interface in stratified Lake Lugano ($0.07\text{--}0.71 \text{ d}^{-1}$, Blees et al. 2014). In Mariager Fjord, rate constants in incubations with $\sim 28 \mu\text{M}$ and $< 50 \text{ nM}$ oxygen (aerobic and anaerobic methane oxidation, respectively) were very similar at each investigated depth (Fig. 4A–E). This contrasts a previous report of methane oxidation in hypoxic coastal waters, where rates were about fivefold lower in incubations with $2\text{--}230 \mu\text{M}$ oxygen compared to $\sim 0.3 \mu\text{M}$ oxygen ($0.2\text{--}0.6$ and $2 \text{ nmol L}^{-1} \text{ d}^{-1}$, respectively; Steinle et al. 2017), and likewise differs from observations of anaerobic methane oxidation from an OMZ (incubations with $< 0.1 \mu\text{M}$ oxygen) where rates were up to 90% inhibited by oxygen concentrations of $1 \mu\text{M}$ and higher (Thamdrup et al. 2019). Furthermore, since rate constants of both aerobic and anaerobic methane oxidation remained relatively constant with depth across the oxic–anoxic interface, the efficiency of either metabolism in the experiments did not appear regulated by the in situ concentration of oxygen.

All three methanotrophic ASVs identified in Mariager Fjord belonged to the Deep Sea-1 clade (Lüke and Frenzel 2011; Tavormina et al. 2015) of the Methylococcales (Fig. 4F–O). The uniform relative abundance of the ASVs across the oxic–anoxic interface was consistent with our observations of similarly invariable rate constants, although relative abundances cannot be converted directly to absolute abundances. The increase in rate constants over time may still suggest that the methanotrophic community was growing. In August, we observed a shift in the dominating ASV from ASV 10 to ASV 23 corresponding to the highest observed rate constants. This

could potentially be related to the intrusion of a different water mass indicated by hydrographic profiles in August (Figs. 2, 3C), although it is unclear how it would contribute to the observed population shift.

Since we did not detect any known anaerobic methanotrophs such as “*Ca. Methyloirabilis*” or ANME, we speculate that members of Deep Sea-1 were responsible for both the aerobic and anaerobic methane oxidation activity observed in our incubations. Their involvement in aerobic methane oxidation is expected, based on genetic potential and observed substrate use of the close relative *M. sedimenti* (Tavormina et al. 2015), however, whether members of the Deep Sea-1 clade are capable of switching from aerobic to anaerobic methane oxidation is not known. Phylogenetic analysis of the three ASVs demonstrated a close relatedness to sequences from other anoxic environments such as Saanich Inlet (Walsh et al. 2009) where the Deep Sea-1 clade primarily occupies the anoxic part of the water column (Torres-Beltrán et al. 2016). The depth interval sampled in Mariager Fjord (4–5 m) was likely too narrow to resolve any redox-driven population distributions. Still, our anaerobic methane oxidation rate data, as well as previously observed depth distributions, strongly suggest that members of the Deep Sea-1 clade are involved in anaerobic methane oxidation. Alternatively, the anaerobic activity could be conducted by as-yet-unrecognized organisms, although this would leave the role of Deep Sea-1 in anoxic water columns unexplained. Indeed, a growing number of studies have identified populations of Methylococcales and other gammaproteobacterial methanotrophs that inhabit the anoxic hypolimnia of stratified lakes and likewise raised the question of the potential for anaerobic metabolisms within these groups (Oswald et al. 2017; Mayr et al. 2020; Rissanen et al. 2021).

Molecular analysis of members of Methylococcales has demonstrated their ability to couple partial denitrification (to NO or N_2O) with methane oxidation (Kits et al. 2015; Oswald et al. 2017; Padilla et al. 2017). Oxygen however still appears required for the first step of methane activation by the particulate methane monooxygenase enzyme, but subsequent oxidation of methanol can be carried out anaerobically (Dam et al. 2013). Whether organisms such as the Deep Sea-1 can fully bypass oxygen by utilizing other electron acceptors like nitrate, nitrite, or other nitrogen intermediates, or otherwise obtain oxygen by alternative means similar to “*Ca. Methyloirabilis*,” are questions that merit attention in future studies. Based on the existing evidence, we therefore hypothesize that the Deep Sea-1 ASVs in Mariager Fjord are facultative anaerobes and conduct anaerobic methane oxidation when oxygen is exhausted. Thus, we predict that they possess enzymatic capabilities for both aerobic and anaerobic methane oxidation, as an adaptation to the dynamic environment near the oxic–anoxic interface in Mariager Fjord.

Table 1. Monthly comparison of methane fluxes and depth integrated methane oxidation rates. Rates were integrated over the 4–5-m depth interval analyzed for rates near the oxic–anoxic interface and are shown for oxic ($\sim 28 \mu\text{M}$ oxygen) and anoxic ($< 50 \text{ nM}$ oxygen) incubations, resulting in, respectively, an aerobic CH_4 sink and an anaerobic CH_4 sink. The vertical flux was estimated by multiplying the methane gradient in bottom waters with the vertical turbulent mixing coefficient, K_z , calculated from the density gradient (see “flux calculations” in methods). No methane flux was detected in May.

Month	Interval for depth integr. (m)	CH_4 flux ($\mu\text{mol m}^{-2} \text{d}^{-1}$)	Aerobic CH_4 sink ($\mu\text{mol m}^{-2} \text{d}^{-1}$)	Anaerobic CH_4 sink ($\mu\text{mol m}^{-2} \text{d}^{-1}$)
May	20–25	-	56	36
Jun	20–25	5.0	139	100
Jul	15–19	8.3	72	66
Aug	14–18	11.2	376	439
Oct	16–19	3.7	358	342

A potential link between anaerobic methane oxidation and nitrogen respiration

In all months with anoxic bottom waters, nitrate and nitrite penetrated below the oxic–anoxic interface and maintained a zone where nitrate and nitrite respiration could dominate (Fig. 3F–J). This zone narrowed with time, which is consistent with a previous observation, where both compounds penetrated below the oxic–anoxic interface in July but were depleted at the oxic–anoxic interface in September and October (Jensen et al. 2009). To investigate whether anaerobic methane oxidation in Mariager Fjord could theoretically be sustained by denitrification, we measured rates of denitrification alongside methane oxidation (Fig. S6). Rates of denitrification at anoxic depths ($0.2\text{--}7.7 \mu\text{mol N}_2 \text{ L}^{-1} \text{ d}^{-1}$) were comparable to previous measurements in Mariager Fjord ($0.5\text{--}2.8 \mu\text{mol N}_2 \text{ L}^{-1} \text{ d}^{-1}$, Jensen et al. 2009). Throughout the study, denitrification rates in Mariager Fjord were approximately ten times higher than rates of anaerobic methane oxidation (Fig. S6). Considering this order of magnitude difference along with the proposed 3 : 4 CH_4 to N_2 stoichiometry of methane oxidation coupled to denitrification from nitrite (Ettwig et al. 2010), it is reasonable to hypothesize that anaerobic methane oxidation in Mariager Fjord is coupled to the denitrification pathway, e.g., to the production of NO or N_2O as seen in some gammaproteobacterial methanotrophs (Kits et al. 2015; Oswald et al. 2017; Padilla et al. 2017), which are closely related to the ones observed here. While sulfate could potentially also serve as electron acceptor for AOM, we find it unlikely that this was the case in our incubations given the absence of ANME archaea, which so far appear critical for sulfate-dependent AOM (Knittel and Boetius 2009).

A robust methane filter composed of aerobic and anaerobic methane oxidation

Although methane always constituted $\leq 2\%$ of the total upward flow of electrons to the oxic–anoxic interface, which was dominated by ammonium and sulfide (Figs. 3F–J, S4A–E), the overall methane gradient steepened between June and October (Fig. 3A–E), suggesting an increased diffusive methane

flux from bottom waters to the oxic–anoxic interface that might cause an increased release to surface waters. In order to evaluate whether methane oxidation near the oxic–anoxic interface could consume the upward methane flux, we estimated the vertical flux of methane due to eddy diffusion and compared it to depth integrated rates of methane oxidation over the 4–5-m depth interval analyzed for rates near the oxic–anoxic interface (Table 1). The flux of methane from sediments and toward the depth interval analyzed for rates was calculated using the gradient from 24–25 m to the deepest sample collected for rate measurements (18–19 m in July–October). In June, when the oxic–anoxic interface was at 24-m depth, the methane flux was calculated across the oxic–anoxic interface (23–25-m depth). Estimated values of K_z in bottom waters varied between 0.002 and $0.008 \text{ cm}^2 \text{ s}^{-1}$ across months in agreement with prior estimates in the system ($0.0078 \text{ cm}^2 \text{ s}^{-1}$, Zopfi et al. 2001; $0.003\text{--}0.014 \text{ cm}^2 \text{ s}^{-1}$, Jensen et al. 2009). For a conservative estimate of the role of methane oxidation, we used $K_z = 0.008 \text{ cm}^2 \text{ s}^{-1}$ for our flux calculations.

Estimated fluxes of methane ranged from 3.7 to $11.2 \mu\text{mol m}^{-2} \text{ d}^{-1}$ between months and were highest in August (Table 1). Fluxes were however always 1–2 orders of magnitude lower than the depth integrated rates of either aerobic or anaerobic methane oxidation ($36\text{--}439 \mu\text{mol m}^{-2} \text{ d}^{-1}$), suggesting that methane oxidation near the oxic–anoxic interface in any month could consume the total upward methane flux. Still, the orders of magnitude imbalance between the calculated source (flux) and sink (integrated rates) implies uncertainties associated with one or both estimates. The transfer of activity observed in killed control incubations (Fig. S5) could result in an overestimate of rates by up to $\sim 13\%$, however, such transfer rates ($5\text{--}51 \mu\text{mol m}^{-2} \text{ d}^{-1}$) would only account for a minor part of the discrepancy. Another possibility is that the eddy diffusivity model does not capture the entire methane flux. This could be due to complex, intrusion-driven mixing patterns at the oxic–anoxic interface, which were indicated by short-term fluctuations in salinity and temperature profiles resulting in nonsteady state conditions in a previous study in Mariager Fjord conducting multiple CTD casts per

day (Zopfi et al. 2001). Given such conditions, which are not visible in a single CTD profile as obtained here, our fluxes would most likely be underestimated. Likewise, a substantial non-diffusive contribution to the methane flux from gas ebullition as reported from the near-by Eckernförde Bay (Lohrberg et al. 2020) cannot be excluded, as the potential occurrence of shallow gas and rising bubbles in Mariager Fjord remains to be investigated. Nevertheless, the observation that each respective methane sink, namely aerobic and anaerobic, exceeded the methane source by factors between 10 and 100 (Table 1) strongly suggests that aerobic and anaerobic methane oxidation near the oxic–anoxic interface, potentially mediated by members of Methylococcales belonging to the Deep Sea-1 clade, can effectively prevent the escape of methane to surface waters and thereby mitigate the effect of the accumulating methane on emissions to the atmosphere. The effectiveness of the filter is further witnessed by the methane concentration minimum, which persisted just above the oxic–anoxic interface (Fig. 3). Thus, we conclude that methane oxidation near the oxic–anoxic interface serves as an effective methane filter independent of ambient oxygen concentrations, which is a feature of particular importance in a shallow and dynamic system such as Mariager Fjord, where oxygen conditions can change rapidly.

Data Availability Statement

Sequence data has been submitted to GenBank under accession number PRJNA749906 and all other data is available from corresponding author upon request.

References

- Abril, G., and N. Iversen. 2002. Methane dynamics in a shallow non-tidal estuary (Randers Fjord, Denmark). *Mar. Ecol. Prog. Ser.* **230**: 171–181. doi:10.3354/meps230171
- Andersen, P., and H. M. Sørensen. 1986. Population dynamics and trophic coupling in pelagic microorganisms in eutrophic coastal waters. *Mar. Ecol. Prog. Ser.* **33**: 99–109.
- Blees, J., and others. 2014. Micro-aerobic bacterial methane oxidation in the chemocline and anoxic water column of deep south-alpine Lake Lugano (Switzerland). *Limnol. Oceanogr.* **59**: 311–324. doi:10.4319/lo.2014.59.2.0311
- Breitburg, D., and others. 2018. Declining oxygen in the global ocean and coastal waters. *Science* **359**: eaam7240. doi:10.1126/science.aam7240
- Brune, A., P. Frenzel, and H. Cypionka. 2000. Life at the oxic–anoxic interface: Microbial activities and adaptations. *FEMS Microbiol. Rev.* **24**: 691–710. doi:10.1111/j.1574-6976.2000.tb00567.x
- Bussmann, I., A. Matousu, R. Osudar, and S. Mau. 2015. Assessment of the radio ^3H -CH₄ tracer technique to measure aerobic methane oxidation in the water column. *Limnol. Oceanogr.: Methods* **13**: 312–327. doi:10.1002/lom3.10027
- Callahan, B. J., P. J. McMurdie, M. J. Rosen, A. W. Han, A. J. A. Johnson, and S. P. Holmes. 2016. DADA2: High-resolution sample inference from Illumina amplicon data. *Nat. Methods* **13**: 581–583. doi:10.1038/nmeth.3869
- Capelle, D. W., S. J. Hallam, and P. D. Tortell. 2019. Time-series CH₄ measurements from Saanich inlet, BC, a seasonally anoxic fjord. *Mar. Chem.* **215**: 103664. doi:10.1016/j.marchem.2019.103664
- Cline, J. D. 1969. Spectrophotometric determination of hydrogen sulfide in natural waters. *Limnol. Oceanogr.* **14**: 454–458. doi:10.4319/lo.1969.14.3.0454
- Dalsgaard, T., B. Thamdrup, L. Fariás, and N. P. Revsbech. 2012. Anammox and denitrification in the oxygen minimum zone of the eastern South Pacific. *Limnol. Oceanogr.* **57**: 1331–1346. doi:10.4319/lo.2012.57.5.1331
- Dam, B., S. Dam, J. Blom, and W. Liesack. 2013. Genome analysis coupled with physiological studies reveals a diverse nitrogen metabolism in *Methylocystis* sp. strain SC2. *PLoS One* **8**: e74767. doi:10.1371/journal.pone.0074767
- De Brabandere, L., B. Thamdrup, N. P. Revsbech, and R. Foadi. 2012. A critical assessment of the occurrence and extend of oxygen contamination during anaerobic incubations utilizing commercially available vials. *J. Microbiol. Methods* **88**: 147–154. doi:10.1016/j.mimet.2011.11.001
- De Brabandere, L., D. E. Canfield, T. Dalsgaard, G. E. Friederich, N. P. Revsbech, O. Ulloa, and B. Thamdrup. 2014. Vertical partitioning of nitrogen-loss processes across the oxic-anoxic interface of an oceanic oxygen minimum zone. *Environ. Microbiol.* **16**: 3041–3054. doi:10.1111/1462-2920.12255
- Diao, M., R. Sinnige, K. Kalbitz, J. Huisman, and G. Muyzer. 2017. Succession of bacterial communities in a seasonally stratified lake with an anoxic and sulfidic hypolimnion. *Front. Microbiol.* **8**: 2511. doi:10.3389/fmicb.2017.02511
- Diaz, R. J., and R. Rosenberg. 2008. Spreading dead zones and consequences for marine ecosystems. *Science* **321**: 926–929. doi:10.1126/science.1156401
- Edgar, R. C. 2004. MUSCLE: Multiple sequence alignment with high accuracy and high throughput. *Nucleic Acids Res.* **32**: 1792–1797. doi:10.1093/nar/gkh340
- Egger, M., and others. 2016. Rapid sediment accumulation results in high methane effluxes from coastal sediments. *PLoS One* **11**: e0161609. doi:10.1371/journal.pone.0161609
- Ettwig, K. F., and others. 2010. Nitrite-driven anaerobic methane oxidation by oxygenic bacteria. *Nature* **464**: 543–548. doi:10.1038/nature08883
- Ettwig, K. F., B. Zhu, D. Speth, J. T. Keltjens, M. S. Jetten, and B. Kartal. 2016. Archaea catalyze iron-dependent anaerobic oxidation of methane. *Proc. Natl. Acad. Sci. USA* **113**: 12792–12796. doi:10.1073/pnas.1609534113

- Fallesen, G., F. Andersen, and B. Larsen. 2000. Life, death and revival of the hypertrophic Mariager Fjord, Denmark. *J. Mar. Syst.* **25**: 313–321. doi:10.1016/S0924-7963(00)00024-5
- Fenchel, T., C. Bernard, G. Esteban, B. J. Finlay, P. J. Hansen, and N. Iversen. 1995. Microbial diversity and activity in a Danish fjord with anoxic deep water. *Ophelia* **43**: 45–100. doi:10.1080/00785326.1995.10430576
- Ferry, J. G. 1992. Biochemistry of methanogenesis. *Crit. Rev. Biochem. Mol. Biol.* **27**: 473–503. doi:10.3109/10409239209082570
- Galloway, J. N., and others. 2008. Transformation of the nitrogen cycle: Recent trends, questions, and potential solutions. *Science* **320**: 889–892. doi:10.1126/science.1136674
- García-Robledo, E., A. Corzo, and S. Papaspyrou. 2014. A fast and direct spectrophotometric method for the sequential determination of nitrate and nitrite at low concentrations in small volumes. *Mar. Chem.* **162**: 30–36. doi:10.1016/j.marchem.2014.03.002
- Gelesh, L., K. Marshall, W. Boicourt, and L. Lapham. 2016. Methane concentrations increase in bottom waters during summertime anoxia in the highly eutrophic estuary, Chesapeake Bay, U.S.A. *Limnol. Oceanogr.* **61**: S253–S266. doi:10.1002/lno.10272
- Gilbert, D., N. N. Rabalais, R. J. Díaz, and J. Zhang. 2010. Evidence for greater oxygen decline rates in the coastal ocean than in the open ocean. *Biogeosciences* **7**: 2283–2296. doi:10.5194/bg-7-2283-2010
- Graf, J. S., and others. 2018. Bloom of a denitrifying methanotroph, '*Candidatus* *Methylomirabilis limnetica*', in a deep stratified lake. *Environ. Microbiol.* **20**: 2598–2614. doi:10.1111/1462-2920.14285
- Graham, D. W., J. A. Chaudhary, R. S. Hanson, and R. G. Arnold. 1993. Factors affecting competition between type I and type II methanotrophs in two-organism, continuous-flow reactors. *Microb. Ecol.* **25**: 1–17. doi:10.1007/BF00182126
- van Grinsven, S., J. S. Sinninghe Damste, A. Abdala Asbun, J. C. Engelmann, J. Harrison, and L. Villanueva. 2020. Methane oxidation in anoxic lake water stimulated by nitrate and sulfate addition. *Environ. Microbiol.* **22**: 766–782. doi:10.1111/1462-2920.14886
- Haroon, M. F., S. Hu, Y. Shi, M. Imelfort, J. Keller, P. Hugenholtz, Z. Yuan, and G. W. Tyson. 2013. Anaerobic oxidation of methane coupled to nitrate reduction in a novel archaeal lineage. *Nature* **500**: 567–570. doi:10.1038/nature12375
- Hirayama, H., and others. 2013. *Methylomarinum vadi* gen. nov., sp. nov., a methanotroph isolated from two distinct marine environments. *Int. J. Syst. Evol. Microbiol.* **63**: 1073–1082. doi:10.1099/ijs.0.040568-0
- Holmes, R. M., A. Aminot, R. Kérouel, B. A. Hooker, and B. J. Peterson. 1999. A simple and precise method for measuring ammonium in marine and freshwater ecosystems. *Can. J. Fish. Aquat. Sci.* **56**: 1801–1808. doi:10.1139/f99-128
- Jensen, M. M., J. Petersen, T. Dalsgaard, and B. Thamdrup. 2009. Pathways, rates, and regulation of N₂ production in the chemocline of an anoxic basin, Mariager Fjord, Denmark. *Mar. Chem.* **113**: 102–113. doi:10.1016/j.marchem.2009.01.002
- Kalyaanamoorthy, S., B. Q. Minh, T. K. Wong, A. von Haeseler, and L. S. Jermiin. 2017. ModelFinder: Fast model selection for accurate phylogenetic estimates. *Nat. Methods* **14**: 587–589. doi:10.1038/nmeth.4285
- Kits, K. D., M. G. Klotz, and L. Y. Stein. 2015. Methane oxidation coupled to nitrate reduction under hypoxia by the Gammaproteobacterium *Methylomonas denitrificans*, sp. nov. type strain FJG1. *Environ. Microbiol.* **17**: 3219–3232. doi:10.1111/1462-2920.12772
- Knief, C. 2015. Diversity and habitat preferences of cultivated and uncultivated aerobic methanotrophic bacteria evaluated based on *pmoA* as molecular marker. *Front. Microbiol.* **6**: 1346. doi:10.3389/fmicb.2015.01346
- Knittel, K., and A. Boetius. 2009. Anaerobic oxidation of methane: Progress with an unknown process. *Annu. Rev. Microbiol.* **63**: 311–334. doi:10.1146/annurev.micro.61.080706.093130
- Lewis, B., and W. Landing. 1991. The biogeochemistry of manganese and iron in the Black Sea. *Deep Sea Res. Oceanogr. Res. Pap.* **38**: S773–S803. doi:10.1016/S0198-0149(10)80009-3
- Lohrberg, A., O. Schmale, I. Ostrovsky, H. Niemann, P. Held, and J. Schneider von Deimling. 2020. Discovery and quantification of a widespread methane ebullition event in a coastal inlet (Baltic Sea) using a novel sonar strategy. *Sci. Rep.* **10**: 4393. doi:10.1038/s41598-020-60283-0
- Lüke, C., and P. Frenzel. 2011. Potential of *pmoA* amplicon pyrosequencing for methanotroph diversity studies. *Appl. Environ. Microbiol.* **77**: 6305–6309. doi:10.1128/AEM.05355-11
- Mau, S., J. Blees, E. Helmke, H. Niemann, and E. Damm. 2013. Vertical distribution of methane oxidation and methanotrophic response to elevated methane concentrations in stratified waters of the Arctic fjord Storfjorden (Svalbard, Norway). *Biogeosciences* **10**: 6267–6278. doi:10.5194/bg-10-6267-2013
- Mayr, M. J., M. Zimmermann, C. Guggenheim, A. Brand, and H. Burgmann. 2020. Niche partitioning of methane-oxidizing bacteria along the oxygen-methane counter gradient of stratified lakes. *ISME J.* **14**: 274–287. doi:10.1038/s41396-019-0515-8
- Minh, B. Q., H. A. Schmidt, O. Chernomor, D. Schrempf, M. D. Woodhams, A. von Haeseler, and R. Lanfear. 2020. IQ-TREE 2: New models and efficient methods for phylogenetic inference in the genomic era. *Mol. Biol. Evol.* **37**: 1530–1534. doi:10.1093/molbev/msaa015

- Miyashita, A., and others. 2009. Development of 16S rRNA gene-targeted primers for detection of archaeal anaerobic methanotrophs (ANMEs). *FEMS Microbiol. Lett.* **297**: 31–37. doi:10.1111/j.1574-6968.2009.01648.x
- Naguib, M. 1976. Stoichiometry of methane oxidation in the methane-oxidizing strain M 102 under the influence of various CH₄/O₂ mixtures. *Z. Allg. Mikrobiol.* **16**: 437–444. doi:10.1002/jobm.3630160604
- Oswald, K., J. Milucka, A. Brand, S. Littmann, B. Wehrli, M. M. M. Kuypers, and C. J. Schubert. 2015. Light-dependent aerobic methane oxidation reduces methane emissions from seasonally Stratified Lakes. *PLoS One* **10**: e0132574. doi:10.1371/journal.pone.0132574
- Oswald, K., and others. 2017. Crenothrix are major methane consumers in stratified lakes. *ISME J.* **11**: 2124–2140. doi:10.1038/ismej.2017.77
- Ovreås, L., L. Forney, F. L. Daae, and V. Torsvik. 1997. Distribution of bacterioplankton in meromictic Lake Saelenvannet, as determined by denaturing gradient gel electrophoresis of PCR-amplified gene fragments coding for 16S rRNA. *Appl. Environ. Microbiol.* **63**: 3367–3373. doi:10.1128/aem.63.9.3367-3373.1997
- Padilla, C. C., and others. 2016. NC10 bacteria in marine oxygen minimum zones. *ISME J.* **10**: 2067–2071. doi:10.1038/ismej.2015.262
- Padilla, C. C., A. D. Bertagnolli, L. A. Bristow, N. Sarode, J. B. Glass, B. Thamdrup, and F. J. Stewart. 2017. Metagenomic binning recovers a transcriptionally active gammaproteobacterium linking methanotrophy to partial denitrification in an anoxic oxygen minimum zone. *Front. Mar. Sci.* **4**: 23. doi:10.3389/fmars.2017.00023
- Ramsing, N. B., H. Fossing, T. G. Ferdelman, F. Andersen, and B. Thamdrup. 1996. Distribution of bacterial populations in a stratified fjord (Mariager Fjord, Denmark) quantified by in situ hybridization and related to chemical gradients in the water column. *Appl. Environ. Microbiol.* **62**: 1391–1404. doi:10.1128/aem.62.10.3915-3915b.1996
- Reeburgh, W. S. 2007. Oceanic methane biogeochemistry. *Chem. Rev.* **107**: 486–513. doi:10.1021/cr050362v
- Reeburgh, W. S., B. B. Ward, S. C. Whalen, K. A. Sandbeck, K. A. Kilpatrick, and L. J. Kerkhof. 1991. Black Sea methane geochemistry. *Deep Sea Res. Oceanogr. Res. Pap.* **38**: S1189–S1210. doi:10.1016/S0198-0149(10)80030-5
- Rissanen, A. J., and others. 2021. Vertical stratification patterns of methanotrophs and their genetic controllers in water columns of oxygen-stratified boreal lakes. *FEMS Microbiol. Ecol.* **97**: fiae252. doi:10.1093/femsec/fiae252
- Rogener, M. K., K. S. Hunter, N. N. Rabalais, B. J. Roberts, A. Bracco, F. J. Stewart, and S. B. Joye. 2021. Pelagic denitrification and methane oxidation in oxygen-depleted waters of the Louisiana shelf. *Biogeochemistry* **154**: 231–254. doi:10.1007/s10533-021-00778-8
- Roland, F. A., A. V. Borges, F. Darchambeau, M. Llorós, J.-P. Descy, and C. Morana. 2021. The possible occurrence of iron-dependent anaerobic methane oxidation in an Archean Ocean analogue. *Sci. Rep.* **11**: 1597. doi:10.1038/s41598-021-81210-x
- Sansone, F. J., B. N. Popp, A. Gasc, A. W. Graham, and T. M. Rust. 2001. Highly elevated methane in the eastern tropical North Pacific and associated isotopically enriched fluxes to the atmosphere. *Geophys. Res. Lett.* **28**: 4567–4570. doi:10.1029/2001GL013460
- Saunois, M., and others. 2020. The global methane budget 2000–2017. *Earth Syst. Sci. Data* **12**: 1561–1623. doi:10.5194/essd-12-1561-2020
- Schubert, C. J., F. Vazquez, T. Lösekann-Behrens, K. Knittel, M. Tonolla, and A. Boetius. 2011. Evidence for anaerobic oxidation of methane in sediments of a freshwater system (Lago di Cadagno). *FEMS Microbiol. Ecol.* **76**: 26–38. doi:10.1111/j.1574-6941.2010.01036.x
- Shirodkar, G., S. W. A. Naqvi, H. Naik, A. K. Pratihary, S. Kurian, and D. M. Shenoy. 2018. Methane dynamics in the shelf waters of the west coast of India during seasonal anoxia. *Mar. Chem.* **203**: 55–63. doi:10.1016/j.marchem.2018.05.001
- Steinle, L., and others. 2015. Water column methanotrophy controlled by a rapid oceanographic switch. *Nat. Geosci.* **8**: 378–382. doi:10.1038/ngeo2420
- Steinle, L., and others. 2017. Effects of low oxygen concentrations on aerobic methane oxidation in seasonally hypoxic coastal waters. *Biogeosciences* **14**: 1631–1645. doi:10.5194/bg-2016-422
- Steinsdóttir, H. G. R., and others. n.d. Anaerobic methane oxidation in a coastal oxygen minimum zone: spatial and temporal dynamics.
- Takai, K., and K. Horikoshi. 2000. Rapid detection and quantification of members of the archaeal community by quantitative PCR using fluorogenic probes. *Appl. Environ. Microbiol.* **66**: 5066–5072. doi:10.1128/AEM.66.11.5066-5072.2000
- Tavormina, P. L., W. Ussler, S. B. Joye, B. K. Harrison, and V. J. Orphan. 2010. Distributions of putative aerobic methanotrophs in diverse pelagic marine environments. *ISME J.* **4**: 700–710. doi:10.1038/ismej.2009.155
- Tavormina, P. L., W. Ussler 3rd, J. A. Steele, S. A. Connon, M. G. Klotz, and V. J. Orphan. 2013. Abundance and distribution of diverse membrane-bound monooxygenase (CUMMO) genes within the Costa Rica oxygen minimum zone. *Environ. Microbiol. Rep.* **5**: 414–423. doi:10.1111/1758-2229.12025
- Tavormina, P. L., R. Hatzepichler, S. McGlynn, G. Chadwick, K. S. Dawson, S. A. Connon, and V. J. Orphan. 2015. *Methyloprofundus sedimenti* gen. Nov., sp. nov., an obligate methanotroph from ocean sediment belonging to the ‘deep sea-1’ clade of marine methanotrophs. *Int. J. Syst. Evol. Microbiol.* **65**: 251–259. doi:10.1099/ijs.0.062927-0
- Thamdrup, B., and T. Dalsgaard. 2002. Production of N₂ through anaerobic ammonium oxidation coupled to nitrate

- reduction in marine sediments. *Appl. Environ. Microbiol.* **68**: 1312–1318. doi:[10.1128/AEM.68.3.1312-1318.2002](https://doi.org/10.1128/AEM.68.3.1312-1318.2002)
- Thamdrup, B., H. G. R. Steinsdóttir, A. D. Bertagnolli, C. C. Padilla, N. V. Patin, E. Garcia-Robledo, L. A. Bristow, and F. J. Stewart. 2019. Anaerobic methane oxidation is an important sink for methane in the ocean's largest oxygen minimum zone. *Limnol. Oceanogr.* **64**: 2569–2585. doi:[10.1002/lno.11235](https://doi.org/10.1002/lno.11235)
- Tiano, L., E. Garcia-Robledo, and N. P. Revsbech. 2014. A new highly sensitive method to assess respiration rates and kinetics of natural planktonic communities by use of the switchable trace oxygen sensor and reduced oxygen concentrations. *PLoS One* **9**: e105399. doi:[10.1371/journal.pone.0105399](https://doi.org/10.1371/journal.pone.0105399)
- Torres-Beltrán, M., A. K. Hawley, D. W. Capelle, M. P. Bhatia, W. E. Durmo, P. D. Tortell, and S. J. Hallamand. 2016. Methanotrophic community dynamics in a seasonally Anoxic Fjord: Saanich Inlet, British Columbia. *Front. Mar. Sci.* **3**: 268. doi:[10.3389/fmars.2016.00268](https://doi.org/10.3389/fmars.2016.00268)
- Torres-Beltrán, M., and others. 2017. A compendium of geochemical information from the Saanich inlet water column. *Sci. Data* **4**: 170159. doi:[10.1038/sdata.2017.159](https://doi.org/10.1038/sdata.2017.159)
- Trotsenko, Y. A., and J. C. Murrell. 2008. Metabolic aspects of aerobic obligate methanotrophy. *Adv. Appl. Microbiol.* **63**: 183–229. doi:[10.1016/S0065-2164\(07\)00005-6](https://doi.org/10.1016/S0065-2164(07)00005-6)
- Turner, A. J., C. Frankenberg, and E. A. Kort. 2019. Interpreting contemporary trends in atmospheric methane. *Proc. Natl. Acad. Sci. USA* **116**: 2805–2813. doi:[10.1073/pnas.1814297116](https://doi.org/10.1073/pnas.1814297116)
- Vaksmaa, A., M. S. Jetten, K. F. Ettwig, and C. Lüke. 2017. *McrA* primers for the detection and quantification of the anaerobic archaeal methanotroph ‘*Candidatus Methanoperedens nitroreducens*’. *Appl. Microbiol. Biotechnol.* **101**: 1631–1641. doi:[10.1007/s00253-016-8065-8](https://doi.org/10.1007/s00253-016-8065-8)
- Valentine, D. L., D. C. Blanton, W. S. Reeburgh, and M. Kastner. 2001. Water column methane oxidation adjacent to an area of active hydrate dissociation, Eel River Basin. *Geochim. Cosmochim. Acta* **65**: 2633–2640. doi:[10.1016/S0016-7037\(01\)00625-1](https://doi.org/10.1016/S0016-7037(01)00625-1)
- Vigneron, A., P. Cruaud, P. Pignet, J.-C. Caprais, M.-A. Cambon-Bonavita, A. Godfroy, and L. Toffin. 2013. Archaeal and anaerobic methane oxidizer communities in the Sonora Margin cold seeps, Guaymas Basin (Gulf of California). *ISME J.* **7**: 1595–1608. doi:[10.1038/ismej.2013.18](https://doi.org/10.1038/ismej.2013.18)
- Walsh, D. A., E. Zaikova, C. G. Howes, Y. C. Song, J. J. Wright, S. G. Tringe, P. D. Tortell, and S. J. Hallam. 2009. Metagenome of a versatile chemolithoautotroph from expanding oceanic dead zones. *Science* **326**: 578–582. doi:[10.1126/science.1175309](https://doi.org/10.1126/science.1175309)
- Weber, T., N. A. Wiseman, and A. Kock. 2019. Global ocean methane emissions dominated by shallow coastal waters. *Nat. Commun.* **10**: 4584. doi:[10.1038/s41467-019-12541-7](https://doi.org/10.1038/s41467-019-12541-7)
- Wiesenburg, D. A., and N. L. Guinasso Jr. 1979. Equilibrium solubilities of methane, carbon monoxide, and hydrogen in water and sea water. *J. Chem. Eng. Data* **24**: 356–360. doi:[10.1021/je60083a006](https://doi.org/10.1021/je60083a006)
- Zopfi, J., T. G. Ferdelman, B. B. Jørgensen, A. Teske, and B. Thamdrup. 2001. Influence of water column dynamics on sulfide oxidation and other major biogeochemical processes in the chemocline of Mariager Fjord (Denmark). *Mar. Chem.* **74**: 29–51. doi:[10.1016/S0304-4203\(00\)00091-8](https://doi.org/10.1016/S0304-4203(00)00091-8)

Acknowledgments

We are grateful to Gert Pedersen, Johannes Christian Thorhauge and Lars Peter Jørgensen for enabling and assisting with sampling in Mariager Fjord, and Anders Soltau Barnewitz, Lene Jakobsen and Louise Reinbach Hansen for help with sampling and chemical analysis. We thank Erik Laursen for carrying out PCR analysis and Carmen Czepe at the Next Generation Sequencing Facility of the Vienna Biocenter (www.vbcf.ac.at) for sequencing. We thank two anonymous reviewers for their constructive comments. This work was supported by the European Research Council (European Research Council (ERC) Advanced Grant 695599 NOVAMOX to BT).

Conflict of Interest

None declared

Submitted 25 August 2021

Revised 14 February 2022

Accepted 14 March 2022

Associate editor: Florence Schubotz